ISSN 1674-1056
http://cpb.iphy.ac.cn
http://iopscience.iop.org/cpb
中国物理 B
Chinese Physics
中国物理 Chinese Physics B

Modulated thermal transport for flexural and in-plane phonons in double-stub graphene nanoribbons

Chang-Ning Pan(潘长宁), Meng-Qiu Long(龙孟秋), Jun He(何军)

Citation: Chin. Phys. B . 2018, 27(8): 088101. **doi:** 10.1088/1674-1056/27/8/088101

Journal homepage: http://cpb.iphy.ac.cn; http://iopscience.iop.org/cpb

What follows is a list of articles you may be interested in

Free-standing, curled and partially reduced graphene oxide network as sulfur host for high-performance lithium-sulfur batteries

Hui-Liang Chen(陈辉亮), Zhuo-Jian Xiao(肖卓建), Nan Zhang(张楠), Shi-Qi Xiao(肖仕奇), Xiao-Gang Xia(夏晓刚), Wei Xi(席薇), Yan-Chun Wang(王艳春), Wei-Ya Zhou(周维亚), Si-Shen Xie(解思深)

Chin. Phys. B . 2018, 27(6): 068101. **doi:** 10.1088/1674-1056/27/6/068101

One-dimensional method of investigating the localized states in armchair graphene-like nanoribbons with defects

Yang Xie(谢阳), Zhi-Jian Hu(胡智健), Wen-Hao Ding(丁文浩), Xiao-Long Lü(吕小龙), Hang Xie(谢航)

Chin. Phys. B . 2017, 26(12): 127310. **doi:** 10.1088/1674-1056/26/12/127310

Band structure and edge states of star-like zigzag graphene nanoribbons

Hong Liu(刘红)

Chin. Phys. B . 2017, 26(11): 117301. **doi:** 10.1088/1674-1056/26/11/117301

Charge susceptibilities of armchair graphene nanoribbon in the presence of magnetic field

H Rezania, F Azizi

Chin. Phys. B . 2016, 25(9): 097303. **doi:** 10.1088/1674-1056/25/9/097303

Tunable thermoelectric properties in bended graphene nanoribbons

Chang-Ning Pan(潘长宁), Jun He(何军), Mao-Fa Fang(方卯发)

Chin. Phys. B . 2016, 25(7): 078102. **doi:** 10.1088/1674-1056/25/7/078102

Modulated thermal transport for flexural and in-plane phonons in double-stub graphene nanoribbons*

Chang-Ning Pan(潘长宁)[1,2], Meng-Qiu Long(龙孟秋)[1,†], and Jun He(何军)[1]

[1] *Hunan Key Laboratory of Super Micro-structure and Ultrafast Process, School of Physics and Electronics, Central South University, Changsha* 410083, *China*

[2] *School of Science, Hunan University of Technology, Zhuzhou* 412008, *China*

(Received 6 February 2018; revised manuscript received 16 May 2018; published online 10 July 2018)

Thermal transport properties are investigated for out-of-plane phonon modes (FPMs) and in-plane phonon modes (IPMs) in double-stub graphene nanoribbons (GNRs). The results show that the quantized thermal conductance plateau of FPMs is narrower and more easily broken by the double-stub structure. In the straight GNRs, the thermal conductance of FPMs is higher in the low temperature region due to there being less cut-off frequency and more low-frequency excited modes. In contrast, the thermal conductance of IPMs is higher in the high temperature region because of the wider phonon energy spectrum. Furthermore, the thermal transport of two types of phonon modes can be modulated by the double-stub GNRs, the thermal conductance of FPMs is less than that of IPMs in the low temperatures, but it dominates the contribution to the total thermal conductance in the high temperatures. The modulated thermal conductance can provide a guideline for designing high-performance thermal or thermoelectric nanodevices based on graphene.

Keywords: graphene nanoribbon, flexural phonons, in-plane phonons, thermoelectric properties

PACS: 81.05.U–, 73.63.–b, 72.20.Pa **DOI:** 10.1088/1674-1056/27/8/088101

1. Introduction

Since it was first discovered several years ago, two-dimensional graphene and quasi-one-dimensional graphene nanoribbons (GNRs) have attracted a great deal of attention due to their extraordinary electronic, thermal, and mechanical properties. It has been predicted to have many potential applications in nanoelectronics, photonics, and optoelectronics, and has been believed to be a promising candidate for next generation electronics.[1–4] As for the thermal properties, many theoretical and experimental researches have been reported in graphene and graphene-based thermal devices. For instance, the thermal rectification efficiencies have been observed in asymmetric graphene ribbons[5] and asymmetric three-terminal graphene nanojunctions,[6] the nonlinear thermal transport and negative differential thermal conductance have been found in graphene nanoribbons,[7] the tuning thermal conductance has been explored in extended defects and folded graphene,[8,9] the enhanced thermoelectric properties[10–15] have also been predicted in graphene-based antidot lattices,[16] edge disorder graphene,[17] kinked graphene nanoribbons,[18,19] and graphene–nanoribbon-based heterojunctions.[20] The phonon thermal conductivities of graphene have been measured by using different experimental methods, and room-temperature values ranging from 600 W/mK to 3000 W/mK have been recorded.[21] In addition, quantized thermal conductance, $\pi^2 k_B^2 T/3h$, which has been observed experimentally in dielectric quantum wires,[22] has also been predicted theoretically in graphene.[23] All of the studied results show that thermal transport properties of graphene always exhibit sensitive structure-dependence such as defects,[24] cavities,[25] and so on. Lattice vibrations in the graphene, as is well known, are characterized by two types of phonons:[26] (i) in-plane phonon modes (IPMs), which vibrate in the plane with linear transverse and longitudinal acoustic branches; (ii) out-of-plane phonon modes, or so-called flexural phonon modes (FPMs), which vibrate out of the plane of the layer. Both types of phonon modes are decomposing in the transport and the thermal conductance can be calculated separately. The exact numerical solution of the phonon Boltzmann equation shows that the lattice thermal conductivity of graphene is dominated by FPMs. A recent theoretical study, which is based on the non-equilibrium Green function (NEGF) approach, also suggests that the FPMs exhibit a significant contribution to the thermal conductivity of graphene.[27] These theoretical results are fully consistent with the experimental measurements of thermal conductivity on both suspended and supported few-layer graphene.[28] However, most of the previous researches thus far investigate the total thermal conductance of the graphene and graphene-based devices, or only focused on the thermal transport properties of FPMs for the graphene. The systematic investigation of two types of phonon modes transport and how to modulate the transport properties

*Project supported by the Science Funds from the Educational Bureau of Hunan Province, China (Grant No. 16C0468), the China Postdoctoral Science Foundation (Grant No. 2016M602421), the Science and Technology Plan of Hunan Province, China (Grant No. 2015RS4002), and the Natural Science Foundation of Hunan Province, China (Grant No. 2015JJ2050).

†Corresponding author. E-mail: mqlong@csu.edu.cn

© 2018 Chinese Physical Society and IOP Publishing Ltd

have been paid less attention.

In the present work, the modulated thermal transport for IPMs and FPMs in double-stub zigzag graphene nanoribbons (ZGNRs) has been simulated in detail by using the NEGF approach.[20] The thermal contributions of IPMs and FPMs are analyzed systematically in the structure. The results show that the cut-off frequency of the 0-th mode of IPMs is considerably larger than that of the FPMs in straight ZGNRs, which yields the low thermal conductance in the low temperature. However, owing to the wider frequency spectrum of IPMs, the thermal conductance of the IPMs is higher than that of the FPMs in the high temperature. In contrast to the straight ZGNRs, both IPMs and FPMs can be modulated effectively by the double-stub structure, some of FPMs have been prohibited to transport in the low frequency range, leading to the low transmission rate and small contribution of FPMs to the whole thermal conductance in the low temperature. However, due to the decreased influence on the high frequency FPMs, the thermal conductance of double-stub ZGNRs is dominated by the FPMs in the high temperature.

2. Model and formulation

The simulated structure is schematized in Fig. 1. It consists of double-stub GNRs section, which acts as a central scattering region, coupled with two semi-infinite ZGNR's leads. The phonon–phonon and electron–phonon interactions, due to the large phonon mean-free path in graphene, are very weak in the considered system,[20,29–32] so the ballistic phonon transports are considered by the NEGF approach.

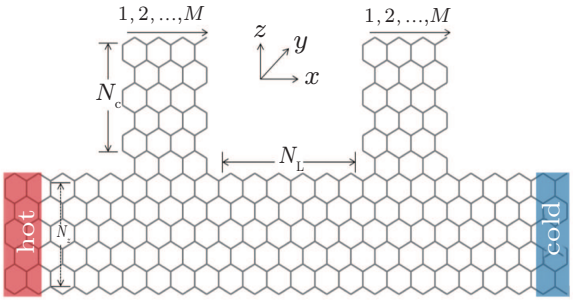


Fig. 1. (color online) Schematic diagram of the double-stub graphene nanoribbons.

In the scheme, the considered structure is divided into three regions: the left/right (L/R) lead and the central scattering region. The force constants between the carbon atoms in different directions can be constructed by using the empirical potential.[33,34] The Hamitonian between IPMs and FPMs is completely decomposed and can be expressed separately as[35]

$$H_\beta = \sum_{\alpha=\mathrm{L,C,R}} H_\beta^\alpha + (u_\beta^{\mathrm{L}})^{\mathrm{T}} V_\beta^{\mathrm{LC}} u_\beta^{\mathrm{C}} + (u_\beta^{\mathrm{C}})^{\mathrm{T}} V_\beta^{\mathrm{CR}} u_\beta^{\mathrm{R}}, \quad (1)$$

where u_β^α is the reduced vibrational displacement of each atom in the α region of β vibration (β is x–y or z). V_β^{LC} and V_β^{CR} are the coupling between center and left/right leads. H_β^α is the linear Hamiltonian for three regions:

$$H_\beta^\alpha = \frac{1}{2}(\dot{u}_\beta^\alpha)^{\mathrm{T}} + \frac{1}{2}(u_\beta^\alpha)^{\mathrm{T}} K_\beta^\alpha u_\beta^\alpha, \quad (2)$$

where K_β^α is the force constant matrix of β vibration. The retarded surface Green function of IPMs and FPMs in the isolated center region and the two (left/right) isolated leads can be calculated as $g_\beta^{\mathrm{r},\alpha} = [(\omega + \mathrm{i}\eta)^2 I - K_\beta^\alpha]^{-1}$, with a constant $\eta \to 0$ and I unit matrix. The retarded self-energy of the leads for IPMs and FPMs, carrying the coupling information between the center region and leads, can be expressed by $\boldsymbol{\Sigma}_\beta^{\mathrm{r},\alpha} = V_\beta^{\mathrm{C}\alpha} g_\beta^{\mathrm{r},\alpha} V_\beta^{\alpha\mathrm{C}}$. The retarded Green's function for the center region connected with leads:

$$\boldsymbol{G}_\beta^{\mathrm{r}} = [(\omega + \mathrm{i}\eta)^2 I - K_\beta^{\mathrm{C}} - \boldsymbol{\Sigma}_\beta^{\mathrm{r,L}} - \boldsymbol{\Sigma}_\beta^{\mathrm{r,R}}]^{-1}. \quad (3)$$

The phonon transmission function and phonon density of states (PDOS) on the i-th atoms in the central region can be derived for IPMs and FPMs:

$$T_\beta(\omega) = \mathrm{Tr}(\boldsymbol{G}_\beta^{\mathrm{r}} \boldsymbol{\Gamma}_\beta^{\mathrm{r,L}} \boldsymbol{G}_\beta^{\mathrm{a}} \boldsymbol{\Gamma}_\beta^{\mathrm{r,R}}), \quad (4)$$

$$\rho_{\mathrm{i},\beta}(\omega) = -\frac{2\omega}{\pi} \mathrm{Tr}(\mathrm{Im}[\boldsymbol{G}_\beta^{\mathrm{r}}]_{\mathrm{ii}}), \quad (5)$$

with the function $\boldsymbol{\Gamma}_\beta^{\mathrm{r},\alpha} = -2\mathrm{Im}\boldsymbol{\Sigma}_\beta^{\mathrm{r},\alpha}$ and the advanced Green function $\boldsymbol{G}_\beta^{\mathrm{a}} = (\boldsymbol{G}_\beta^{\mathrm{r}})^\dagger$. After obtaining the transmission function of the systems, the corresponding thermal conductance contributed from the IPMs or the FPMs can be derived as

$$\kappa_\beta = \frac{\hbar^2}{2\pi k_{\mathrm{B}} T^2} \int_0^\infty \omega^2 \frac{\mathrm{e}^{\hbar\omega/k_{\mathrm{B}}T}}{(\mathrm{e}^{\hbar\omega/k_{\mathrm{B}}T} - 1)^2} T_\beta(\omega) \mathrm{d}\omega, \quad (6)$$

with k_{B} the Boltzmann constant.

3. Numerical results and discussion

Figure 2(a) displays the phonon transmission coefficients of IPMs and FPMs in the straight ZGNRs with width $N_z = 6$ (6-ZGNR). We note that the transmission coefficients of the long-wavelength phonon take the quantized value 2 for IPMs and 1 for FPMs in the limit $\omega \to 0$, which means only the two lowest IPMs (the coupling transversal acoustic and longitudinal acoustic modes) and the lowest FPM are excited. The resulting total transmission coefficient is 3. The transmission curves for IPMs and FPMs appear with the perfect stepwise structure. It is shown that, with the increase of frequencies, the higher acoustic phonon modes are excited and go through smoothly to the straight ZGNRs.

However, the cut-off frequency of both phonon modes have obviously different characteristics. For the 0-th mode, the cut-off frequency is about 180 cm^{-1} for IPMs, which is two times wider than the FPMs about 96 cm^{-1}. The several other foremost lowest frequencies FPMs always have lower cut-off frequencies. The low cut-off frequency means that the phonon modes can be excited more easily. Consequently, in

the low frequency region, the FPMs can be excited firstly and result in a higher phonon transmission rate. In contrast, in the high frequency region, more phonon modes have been excited and the phonon transmission rate of IPMs is higher due to the wider phonon energy spectrum scope: ranged from zero to 1608 cm^{-1} for IPMs while only 906 cm^{-1} for FPMs.

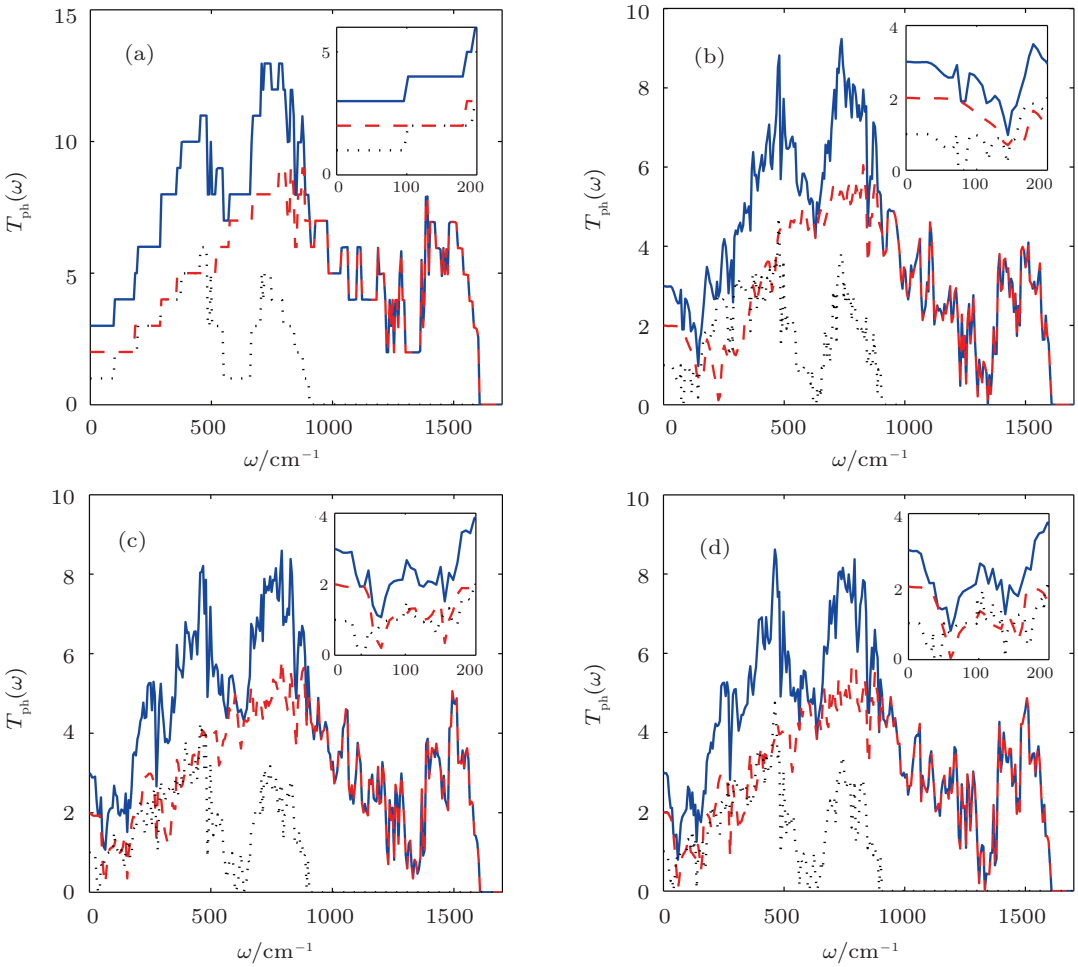


Fig. 2. (color online) Phonon transmission functions for (a) the straight 6-ZGNR; (b) double-stub GNR $N_z = 6$, $N_c = 2$, $N_L = 6$, and $M = 4$; (c) $N_z = 6$, $N_c = 6$, $N_L = 6$, and $M = 4$; and (d) $N_z = 6$, $N_c = 6$, $N_L = 13$, and $M = 4$. The solid, dashed, and dotted curves correspond to the total transmission rate, the transmission rate of IPMs, and the transmission rate of FPMs, respectively.

In Figs. 2(b)–2(d), we describe the calculated transmission rates of various types of double-stub GNRs. It can be found that the transmission rates for both IPMs and FPMs are decreased drastically due to the scattering of the double stubs. Furthermore, the scattering can be modulated by the height of stubs and length between two stubs. The scattering is stronger when the stub is higher, the decrease of transmission rate is also more severe. Comparing the transmission rate of IPMs with that of FPMs, we find that the scattering on the FPMs is much stronger than that of the IPMs in the low frequency region. As shown in the inset in Fig. 2(b), a clear transmission dip appears in the range of frequency from $\omega = 74$ cm^{-1} to $\omega = 86$ cm^{-1}, which suggests the phonon transports of FPMs in the frequencies have been fully scattered by the structure. Such strong scatterings result in that the transmission of FPMs is obviously lower than on IPMs. To elucidate the physical mechanism, we calculate the phonon density of states (PDOS) for both the FPM and IPM at $\omega = 76$ cm^{-1}, as shown in Fig. 3. We find that the phonon of the FPM is completely separate from each other and localize highly on the top of two stubs and at both ends of the structure (as shown in Fig. 3(a). The separate distributions suppress effectively the transport of the phonon and leads to the low transmission rate. However, the PDOS of the IPM is delocalized over the whole system. The well-distributed phonon modes, the same as the pentagon-heptagon defect[35] and the cavities,[24] result that the incoming phonon of the IPM can pass through the system with less scattering. The resulting transmission rate of IPMs is only slightly degraded by this structure and the transport is more robust for IPMs in the low frequency region.

Now, we turn to investigate the thermal conductance of the system. Owing to the decoupling of the FPMs with the IPMS, so the thermal conductance contribution from two kinds of modes can be separated from the total thermal conductance. In Fig. 4, we plot separately the thermal conductance of each kind of mode as a function of temperature T. We find that all of

the thermal conductances increase monotonically with the increase of the temperature; this is because the higher modes are excited with the increasing temperature. However, there exist distinct differences for the contributions of FPMs and IPMs to the total thermal conductance. For the straight ZGNR (6-ZGNR), the thermal conductance of the FPMs is slightly larger than that of the IPMs in the temperature region $T < 138$ K, and then less than that of the IPMs in the high temperature region. The reason is that a lower cut-off frequency exists for the FPMs in the low temperature. So these low-frequency FPMs can be excited easily and contribute to the thermal conductance. However, in the high temperature region, owing to the wider phonon transmission spectrum for IPMs, the more phonon modes of high frequency IPMs are excited and result in the higher thermal conductance. However, for the double-stub GNRs, it is interesting to note that the thermal conductances of IPMs are firstly higher than those of the FPMs in the low temperature region, and then they exhibit a lower thermal conductance value in the high temperature region, as shown in Figs. 4(b)–4(d). It is suggested that the thermal conductance of FPMs and IPMs have been modulated by the double-stub structures. The modulation of thermal conductance stems from the frequency-dependent scattering strength of the IPMs and FPMs. The stubs exhibit much stronger scattering effects for the FPMs in the low frequency region. This can be clearly understood from the PDOS in Fig. 3(a).

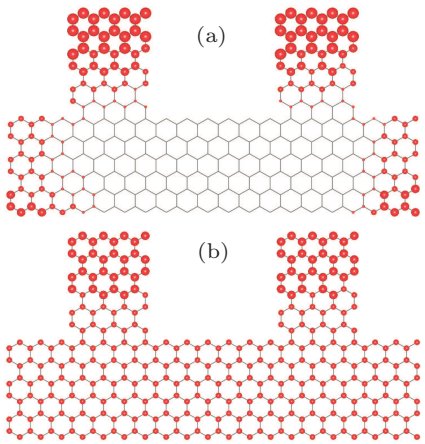


Fig. 3. (color online) The PDOS of the FPMs (a) and the IPMs (b) at $\omega = 76$ cm^{-1} for the double-stub GNR $N_z = 6$, $N_c = 6$, $N_L = 6$, and $M = 4$.

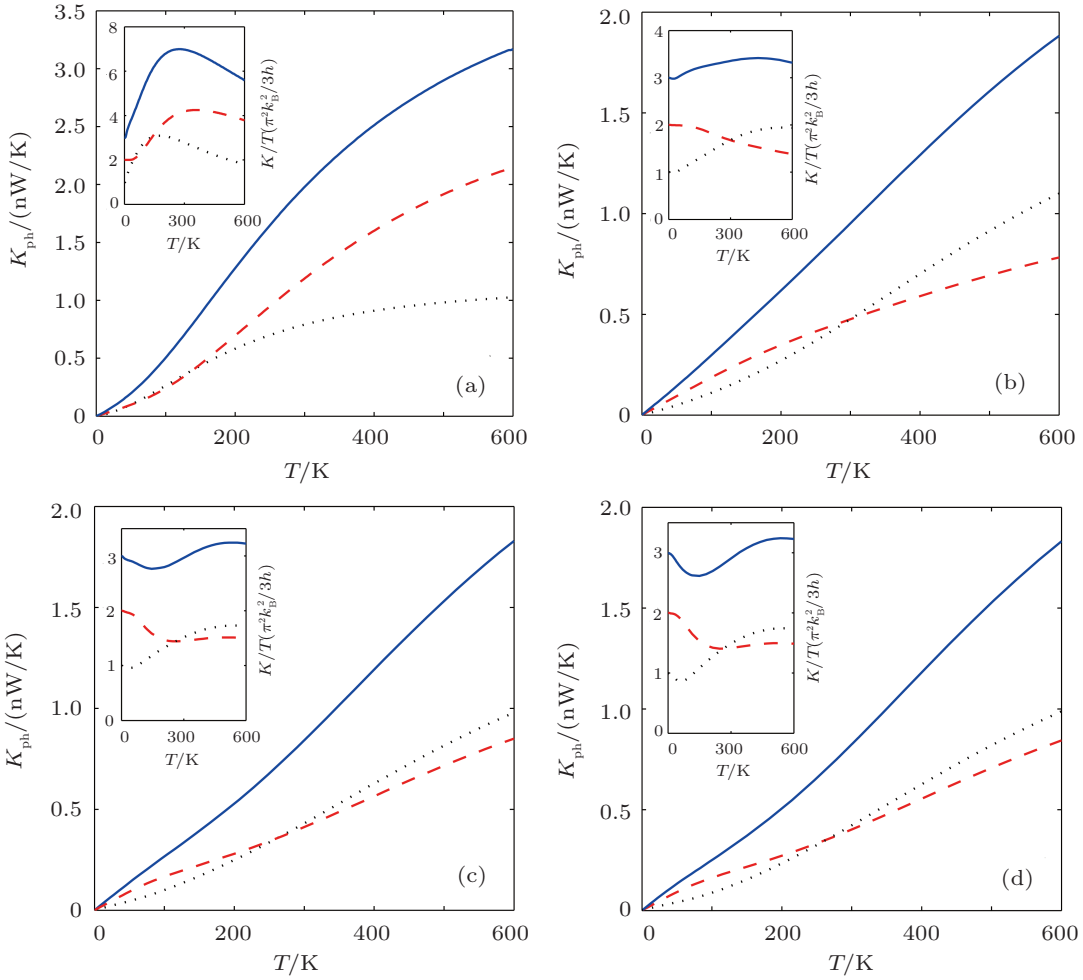


Fig. 4. (color online) The thermal conductance and reduced thermal conductance (insets) as functions of the temperature for (a) the straight 6-ZGNR; (b) double-stub GNR $N_z = 6$, $N_c = 2$, $N_L = 6$, and $M = 4$; (c) $N_z = 6$, $N_c = 6$, $N_L = 6$, and $M = 4$; and (d) $N_z = 6$, $N_c = 6$, $N_L = 13$, and $M = 4$. The solid, dashed, and dotted curves correspond to the total thermal conductance and reduced thermal conductance (insets), the thermal conductance and reduced thermal conductance (insets) of IPMs, and the thermal conductance and reduced thermal conductance (insets) of FPMs, respectively.

The phonons of FPMs are highly localized by the scattering of stubs, and many low frequency FPMs have been entirely scattered by the stubs, which obstruct the heat flow and result in the low thermal conductance. Owing to the delocalization PDOS of IPMs as shown in Fig. 3(b), the heat can flow smoothly through the system, so the relevant thermal conductance is higher. However, for the wider energy spectrum, the scatterings are stronger for IPMs in the high frequency, which suppress effectively the phonon transport and decrease considerably the IPMs thermal conductance in the high energy region.

As shown in the insets of Fig. 4, we demonstrate the temperature dependence of the reduced thermal conductance. It can be found that the reduced thermal conductance of the double-stub GNRs, the same as the straight GNRs, approaches the quantum value 2 ($\pi^2 k_B^2 T/3h$) for IPMs and 1 ($\pi^2 k_B^2 T/3h$) for FPMs in the low temperature limit.[36,37] This can be well understood from the formula $T = \hbar\omega/k_B = hc/K_B\lambda$, which describes the relationship between phonon wavelength and temperature.[38] When $T \to 0$, only the 0-th modes are excited, the wavelength of the phonons is much larger than the dimension of the central scattering region. Therefore, the long-wavelength phonons can be transported perfectly in the double-stub GNRs. Meanwhile, we find that the quantized plateau $2\pi^2 k_B^2 T/3h$ of IPMs is wider and not easily broken by the stub-GNRs. It originates from the fact that the excited frequency of the second IPM (about 180 cm^{-1}) is much larger than that of the second FPM (about 96 cm^{-1}). Instead, the narrow cut-off frequency of FPMs results in the higher FPMs being excited easily with the increase of temperature. Accordingly, the scattering of FPMs becomes stronger due to the higher frequency and the shorter wavelength. So the reduced thermal conductances of FPMs display an obvious dip for the double-stub GNRs in the low energy region. The dip becomes bigger with the increase of stub height (N_c), as shown in the insets of Figs. 4(b) and 4(c).

The FPMs are important for thermal transport of graphene; we calculate the temperature dependence of the contribution for these modes to the total thermal conductance, as shown in Fig.5. In the low temperature limit, $T \to 0$, the thermal contributions come from the perfect transport of three lowest acoustic modes: two coupling lowest transversal acoustic and longitudinal acoustic modes and the lowest FPM. So the contribution of the FPM is always $1/3$ for the straight graphene or stub GNRs. When the temperature is increased but still low, the contribution of FPMs rapidly increases and dominates the thermal conductance for the straight GNRs in the low temperature region. It is because more low-frequency FPMs have been excited for the narrow cut-off frequency and contribute to the thermal transport; however, the contribution of FPMs goes down and is less than 50% in the high temperature region due to the wider phonon energy spectrum scope and the more high-frequency excited modes of IPMs. For the double-stub structure, a big dip occurs in the contribution curve, as shown in the inset in Fig. 5. This phenomenon stems from localized PDOS of FPMs (as shown in Fig. 3(a)) and the extraordinary scattering for FPMs in the low temperature region. However, the contribution of FPMs dominates the thermal conductance in the high temperature. This contribution is more than 50% at the room temperature. Furthermore, the contribution ratio can be modulated by the geometry detail of the structure. Compared with the FPMs, the reversal thermal contribution suggests that the scattering of the stub structure is stronger for IPMs in the high energy region.

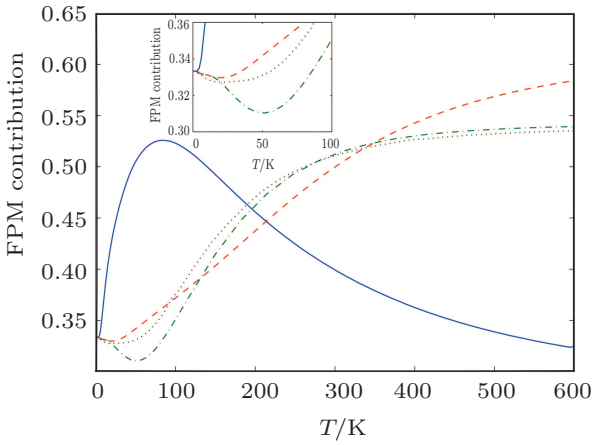


Fig. 5. (color online) The contribution of the thermal conductance of FPMs to the total thermal conductance as functions of temperature. The solid, dashed, dotted, and dash-dotted curves correspond to (a) the straight 6-ZGNR; (b) double-stub GNR $N_z = 6$, $N_c = 2$, $N_L = 6$, and $M = 4$; (c) $N_z = 6$, $N_c = 6$, $N_L = 6$, and $M = 4$; and (d) $N_z = 6$, $N_c = 6$, $N_L = 13$, and $M = 4$, respectively.

4. Conclusion

In conclusion, we have presented an atomistic simulation of the ballistic thermal transport properties of the IPMs and FPMs in the double-stub GNRs. The results show that, owing to the narrow cut-off frequency, the FPMs play an important role in the thermal transport of straight GNRs in the low temperature region; however, in the high temperature region, the IPMs dominate the contribution to the total thermal conductance due to the wider phonon energy spectrum scope and the more excited IPMs contributed to the thermal transport. Compared with the straight GNRs, the double-stub GNRs present the stronger scattering for the FPMs in the low frequency region and a phonon transport dip appears, where the contribution to total thermal conductance is less than the IPMs. Nevertheless, the contribution of FPMs dominates the total thermal conductance in the high temperature region.

References

[1] Geim A K 2009 *Science* **324** 5934
[2] Zhang D, Long M Q, Zhang X J, Ouyang J and Xu H 2016 *RSC Adv.* **6** 15008
[3] Cui L L, Long M Q, Zhang X J, Li X M, Zhang D and Yang B C 2016 *Phys. Lett. A* **380** 730
[4] Zhang D, Long M Q, Zhang X J and Xu H 2015 *RSC Adv.* **5** 96455
[5] Yang N, Zhang G and Li B W 2009 *Appl. Phys. Lett.* **95** 033107
[6] Xie Z X, Li K M, Tang L M, Pan C N and Chen K Q 2012 *Appl. Phys. Lett.* **100** 183110
[7] Hu J, Wang Y, Vallabhaneni A, Ruan X L and Chen Y P 2011 *Appl. Phys. Lett.* **99** 113101
[8] Huang H Q, Xu Y, Zou X L, Wu J and Duan W H 2013 *Phys. Rev. B* **87** 205415
[9] Ouyang T, Chen Y P, Xie Y, Stocks G M and Zhong J X 2011 *Appl. Phys. Lett.* **99** 233101
[10] Wang Q, Xie H Q, Jiao H J, Li Z J and Nie Y H 2012 *Chin. Phys. B* **21** 117310
[11] Wu Z H, Xie H Q, Zhai Y B, Gan L H and Liu J 2015 *Chin. Phys. B* **24** 034402
[12] Yu Z, Guo Y, Zheng J and Chi F 2013 *Chin. Phys. B* **22** 117303
[13] Feng S K, Li S M and Fu H Z 2014 *Chin. Phys. B* **23** 117202
[14] Guo H H, Yang T, Tao P and Zhang Z D 2014 *Chin. Phys. B* **23** 017201
[15] Xue L, Xu B and Yi L 2014 *Chin. Phys. B* **23** 037103
[16] Gunst T, Markussen T, Jauho A P and Brandbyge M 2011 *Phys. Rev. B* **84** 155449
[17] Sevincli H and Cuniberti G 2010 *Phys. Rev. B* **81** 113401
[18] Huang W, Wang J S and Liang G 2011 *Phys. Rev. B* **84** 045410
[19] Liang L, Eduardo C S, Eduardo C G and Vincent M 2012 *Phys. Rev. B* **86** 115438
[20] Pan C N, Xie Z X, Tang L M and Chen K Q 2012 *Appl. Phys. Lett.* **101** 103115
[21] Seol J, Jo I, Moore A, Lindsay L, *et al.* 2010 *Science* **328** 213
[22] Schwab K, Henriksen E A, Worlock J M and Roukes M L 2000 *Science* **404** 974
[23] Yamamoto T and Watanabe K 2004 *Phys. Rev. B* **70** 245402
[24] Xie Z X, Chen K Q and Duan W H 2011 *J Phys: Condens. Matter* **23** 315302
[25] Peng X F, Wang X J, Gong Z Q and Chen K Q 2011 *Appl. Phys. Lett.* **99** 233105
[26] Lindsay L, Broido D A and Mingo N 2010 *Phys. Rev. B* **82** 115427
[27] Lu Y and Guo J 2012 *Phys. Rev. B* **101** 043112
[28] Wang L Z, Xie R G, Bui C T, Liu D, *et al.* 2011 *Nano. Lett.* **11** 113
[29] Ghosh S, Calizo I, Teweldebrhan D, *et al.* 2008 *Appl. Phys. Lett.* **92** 151911
[30] Liu Y Y, Zhou W X, Tang L M and Chen K Q 2013 *Appl. Phys. Lett.* **103** 263118
[31] Zhou W X, Chen K Q, Tang L M and Yao L J 2013 *Phys. Lett. A* **377** 3144
[32] Liu Y Y, Li B L, Chen S Z, Jiang X W and Chen K Q 2017 *Appl. Phys. Lett.* **111** 133107
[33] Brenner D W, Shenderova O A, Harrison J A, *et al.* 2002 *J. Phys.: Conden. Matter* **1** 4
[34] Zimmermann J, Pavone P and Cuniberti G 2008 *Phys. Rev. B* **78** 045410
[35] Tan S H, Tang L M, Xie Z X, Pan C N and Chen K Q 2013 *Carbon* **65** 181
[36] Jiang B, Zhou Y H, Chen C Y and Chen K Q 2015 *Org. Electron.* **23** 133
[37] Chen Q, Tang L M, Chen K Q and Zhao H K 2013 *J. Appl. Phys.* **114** 084301
[38] Sun Q F, Yang P and Guo H 2002 *Phys. Rev. Lett.* **89** 175901